arXiv:1610.06218v1 [cs.RO] 19 Oct 2016

Dynamical Behavior Investigation and Analysis of Novel Mechanism for Simulated Spherical Robot named "RollRoller"

Seyed Amir Tafrishi[a], Sandor M. Veres[a], Esmaeil Esmaeilzadeh[b,*], Mikhail Svinin[c]

[a] *Automation and Control Systems Department, University of Sheffield, Sheffield , UK.*
[b] *Mechanical Engineering Department, University of Tabriz, Tabriz, Iran*
[c] *Mechanical Engineering Department, Kyushu University, Fukuoka, Japan*

Abstract

This paper introduces a simulation study of fluid actuated multi-driven closed system as spherical mobile robot called "RollRoller". Robot's mechanism design consists of two essential parts: tubes to lead a core and mechanical controlling parts to correspond movements. Our robot gets its motivation force by displacing the spherical movable mass known as core in curvy manners inside certain pipes. This simulation investigates by explaining the mechanical and structural features of the robot for creating hydraulic-base actuation via force and momentum analysis. Next, we categorize difficult and integrated 2D motions to omit unstable equilibrium points through derived nonlinear dynamics. We propose an algorithmic position control in forward direction that creates hybrid model as solution for motion planning problem in spherical robot. By deriving nonlinear dynamics of the spherical robot and implementing designed motion planning, we show how RollRoller can be efficient in high speed movements in comparison to the other pendulum-driven models. Then, we validate the results of this position control obtained by nonlinear dynamics via Adams/view simulation which uses the imported solid model of RollRoller. Lastly, We have a look to the circular maneuver of this robot by the same simulator.

Keywords: Spherical mobile robot, mechanism, hydraulic actuation, nonlinaer dynamics, Adams/View simulation, instability region.

1. Introduction

Mobile robots have involved in many new scientific discussions in planetary and field researches during these centuries. For instance, these robots can work

*Corresponding author
Email addresses: amirtafrishi@yahoo.com (Seyed Amir Tafrishi), s.veres@sheffield.ac.uk (Sandor M. Veres), esmzadeh@tabrizu.ac.ir (Esmaeil Esmaeilzadeh), svinin@mech.kyushu-u.ac.jp (Mikhail Svinin)

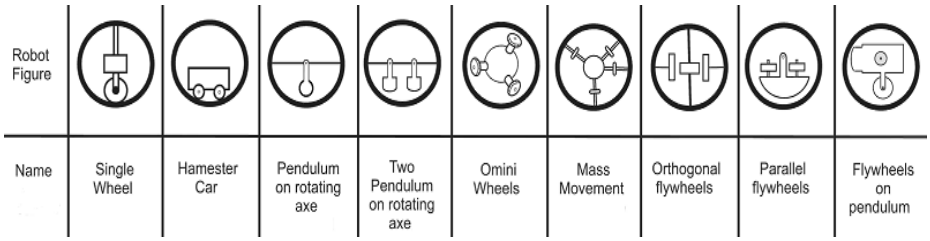

Fig. 1: Previous SMR models.

in hard conditions at hazardous fields. Spherical mobile robots(SMR) as one of the most capable but highly complicated models have been being widely well-known among early researches and innovations for their specific characteristics. SMR's coverage as a ball-like symmetric shell gives diverse capabilities for overcoming limitations in robots with legs, wheels or other types, and makes it tolerable under serious environmentally problematic situation like humid, watery, or even toxic areas [1]. As an initial motivation, NASA scholars developed SMR called Tumbleweeds rover for outer space explorations and they reason how it can be tolerable under challenging conditions and have economic advantages [2].

The rolling sphere controllability was analyzed first theoretically in 1990 [3]. Haleme et al [4] presented the first method for spherical robot motion control via kinematics, where a robot had mono-directional turning wheel (see Fig. 1). Using the tiny car inside the ball shape shell was introduced, [5] whereas, likelihood of losing control of the robot was considerably high. Also, this robot was consuming majority of space inside the ball. After the torque-reaction base internal driving units, some models were developed to excite the SMRs by angular momentum forces. Robot containing rotating internal gyroscope with two motor drivers for each direction named Gyrover was invented [6] as an example. Bhattacharya and Agrawal [7] also suggested perpendicular pair of rotors as alternative internal driving unit. The August robot was reproduced by Javadi in 2002 [8]. This model was making its motivation force solely through unbalancing the center of mass with replacing masses in different axis via rods. "Gyrosphere robot" [9] was introduced by Schroll from MIT in 2008 which it was utilizing both angular momentum and torque-reaction as hybrid system in SMR models. Although, pendulum-driven spherical robots have become common like BYQ-3 [10] model in most known research areas, they could not manage to refine some crucial drawbacks such as limited velocity, unstable points and fully occupied inner space. VolVot [11] and Omnicron [12] are the recently developed robots inspired by the previous SMR models to create hybrid locomotion forms. In addition, there have been many works in advancement of previous SMRs' motion planning by geometric phases [13, 14, 15], algorithm-base [16, 17] and other control methods [18, 19]. The literature review of SMRs proves the discrete and perfunctory researches on various internal driving unit methodologies to actuate ball-shaped robots. This means there is still no unique designed model

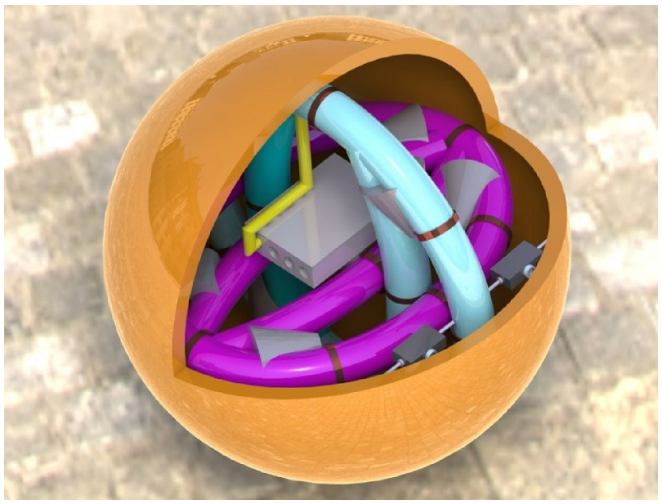

Fig. 2: "RollRoller", spherical mobile robot.

that satisfies all the characteristics for the ideal field research in current SMRs.

In this paper, we introduce a novel spherical mobile robot named "RollRoller" (see Fig. 2). The principle contribution of this paper is validating the 4 degree of freedom unique mechanism (it actuates with angular momentum, gravitational and torque-reaction forces) from derived nonlinear dynamics and numerical simulation. RollRoller moves the core in circular and elliptic pipes in itself to create its motivation force. The required force is produced by circulating the incompressible fluid using hydraulic system. The benefits of this study include:

• The 4 degrees of freedom (e.g., forward/backward, lateral, orientation or jumping abilities) in system is formed parallel with isolated internal driving unit that creates the space for research/rescue tools. We demonstrate our safe hydraulic-base actuator and robot's mechanisms with their characteristics in Section II.

• The unstable point existing in pendulum-like driving models (gravitational-base and torque-reaction drivers) as major problem is omitted due to the model of RollRoller. The classifications of instability and algorithmic control for forward locomotion are analyzed and designed in Section III.

• Ability to have motion planning by using hybrid nonlinear dynamics and showing how it outperforms its counterpart. In Section IV, we derive the nonlinear dynamics and check the robot about its validity for designed criteria and algorithm performance.

• Finally, it is demonstrated (see Section V) how this robot with proposed algorithmic approach can have improvements in backward jumping, fluctuations in velocity and linearity of locomotion in Adams/View simulation. Additionally, we have looked to turning action in 3D plain in different frameworks.

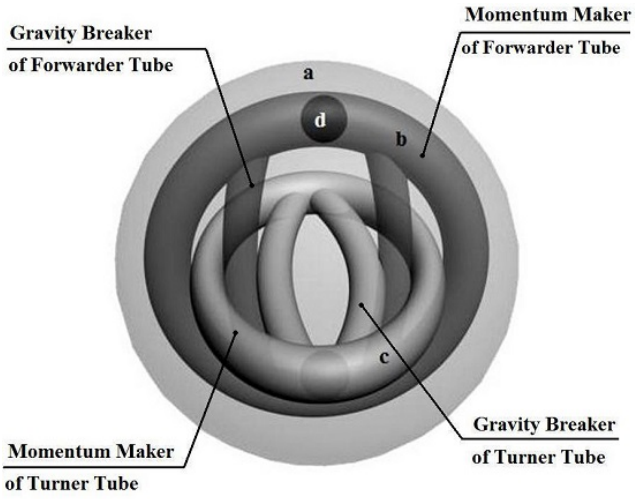

Fig. 3: a. Spherical Shell, b. Forwarder tube, c. Turner tube. d. Copper core.

2. Physical Feature

2.1. Frame of Robot

RollRoller is covered by plastic glass shell like Fig. 3-a. We use pipe-like objects for producing gravity-driven movement force in isolation as a frame and this specification let us to reach flexible mechanism. These tubes are made of polyethylene with high density. Therefore, stamina opposed to unpredicted vibration is neglected and electrical or electromagnetic distortion is impenetrable. In a proposed robot, two groups of these objects are chosen. Main group object is called forwarder tube (FT), placed on striated toward the ground. Next turner tube (TT) is located 90^o tilt to the forwarder tube. For preventing intersection of two objects, the structure of turner tube is made with specific functional change. Accordingly, forwarder tube frame is circular ring. And, turner tube is in elliptic model with certain difference (see Fig. 3). Combined pipes in each tube have names as their roles in machine. For example, the pipes in shape of half-circle are called momentum maker (MM) lines, however, MM at TT with slightly bend structure (non-circular) is also considered as MM. Gravity breaker (GB) is for the half-elliptic pipes. This configuration difference is based on preventing the intersection of paths of the cores in two tubes (FT,TT). Because the sizes and materials of the leading pipes and also the cores are homogeneous, this mutation is assumed for applying all the required moments from the physical and application point of view. Basically, in both FT and TT, the GBs are inner pipes with shortest distances. We call them MM pipes, because they function in creating the required force to move sphere and conversely GB acts as negative impact rectifier which will be studied in next sections.

For each tube, ball-shaped core with constrained mass m_c is placed. These cores surfaces are covered with copper layer and filled with high density materials

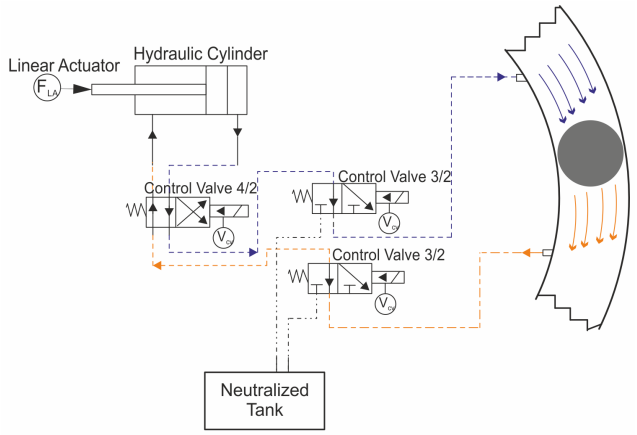

Fig. 4: Schematic of internal driving unit.

(e.g., tungsten or composite steel). Sphere total mass is M_s without including the cores masses. With $m^* = \frac{m_c}{M_s}$, we have:

$$\frac{1}{10} \leq m^* < \frac{1}{3} \tag{1}$$

The reason of constraints in the inequality (1) will be discussed in Section IV.B which it gives the core ability to locate itself in the unstable equilibrium points. By displacement of these cores inside tubes, the required motion is reachable for the total sphere.

2.2. Mechanical Parts

2.2.1. Motion Generator by Hydraulic System

For giving corresponded force to the core, high density flow like superfluid is created by multi-function linear actuators linked to hydraulic cylinder as Fig. 4.

In this system, hydraulics will not be used as actuator instead they are the impulsive fluid replacer without requiring pressurized tank, compressor and pressure regulator inside internal driving unit. The reason is that the total features and internal driving unit mechanism are placed in closed system. The flow is circulated through pipes, hydraulic cylinders and neutralized tank. In this system neutralized tank is responsible to keep fluid in itself and stop it to enter a cylinder in certain times. This happens when fluid flow has certain speed and it may waste energy or oppose the hydraulic actuator task to enforce linear actuator unwillingly. To understand efficiency and required input force to move the core, we assume that core is in a position with maximum gravitational effect F_w and there is certain available static friction between core and pipe F_f (see Fig. 5). The F_B and $F_{\triangle P}$ stands for buoyancy force and created force due

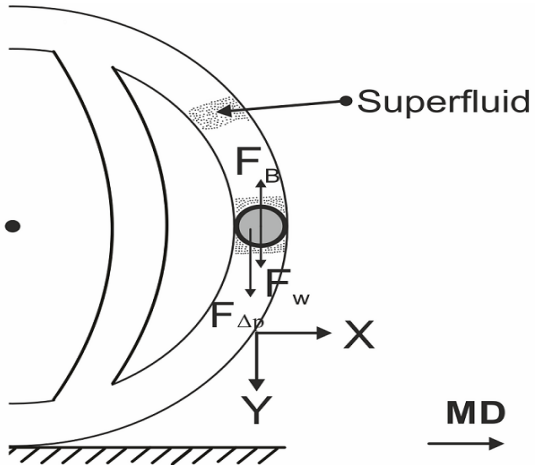

Fig. 5: External force analysis in the maximum resultant condition.

to pressure difference of fluid in core's upper and lower bond. In y direction we have:

$$F_{c_{Max}} = F_w + F_{\triangle P} - F_B - F_f \tag{2}$$

Where m_{lc} and m_b are the masses of the core and displacing fluid. Taking into consideration if superfluid is used inside pipes, the viscosity tends to the negligible value hence F_f is ignored.

$$F_{c_{Max}} = F_w + F_{\triangle P} - F_B = (m_{lc} - m_b)g + \triangle P A_c = m_c g + \triangle P A_c \tag{3}$$

Where m_c is apparent mass of core and A_c is the projection of core area which is perpendicular to y direction. $\triangle P$ tells the efficient pressure difference of the bottom and top of the core inside the pipe. From Eq.(4) the transmitted force from linear actuator to core under the condition that the fluid is in incompressible condition is obtained. The pressure inside the system is considered to be enough to have our operation in perfect manner. The pure enforced motivation toward core is created from sum of both $P_U = \frac{4F_{LA}}{\pi(D_1^2 - D_2^2)}$ and $P_L = \frac{4F_{LA}}{\pi D_1^2}$ as upper and lower chamber created pressure from hydraulic cylinder connect to linear actuator (i.e. F_{LA} is input force of linear actuator). The D_1 and D_2 stand for the full bore piston diameter and piston rod diameter of cylinder, respectively.The r_c is the radius of the core. Due to both sides support in locomotion of core, the pressures are summed to result the total active force as Eq. (4).

$$F_{c_T} = 8r_c^2 F_{LA}[\frac{2D_1^2 - D_2^2}{D_1^2(D_1^2 - D_2^2)}] \tag{4}$$

As a result, to have the core in movable condition with certain accuracy and efficiency, Eq. (5) has to be satisfied. Moreover, Eq. (5) stays applicable when

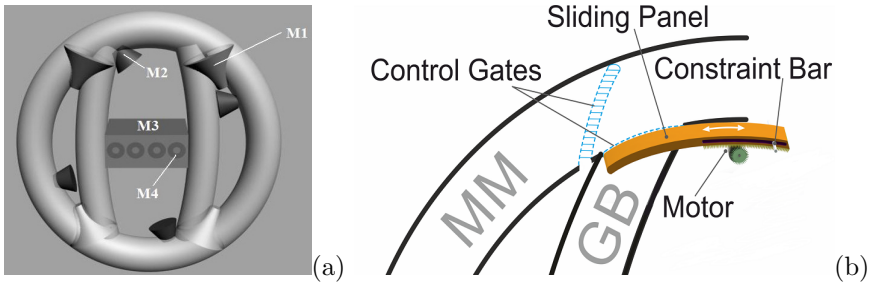

Fig. 6: (a) Connected mechanical instruments. M1. Control gate module M2. Input hole for fluid entrance M3. Motor box M4.Output of fluid, (b) Sliding control gates.

the leakage from one side of the core to other side is insignificantly small (tangent surfaces between sphere-core).

$$F_{c_T} > F_{c_{Max}} \tag{5}$$

This produced fluid force enters the tubes with steady magnitude under ideal condition. However, main goal is to keep cores in certain speed hence fluid actuated force can be vary manually. In Fig. 6 (a) the internal driving unit is placed inside a box and output ports are located on the box in the robot. These systems can perform in either suction or injection function. For each forwarder tube and turner tube, four motors separately are placed in motor boxes. Each of boxes contains four manual input holes connected to specific places on tube as seen in picture. This overall system has got a capability of controlling the core in most variety of control algorithms.

2.2.2. Control Gates

Control gate modules are located in accurate places around the tube for controlling path of the core via opening and closing. Fig. 6 (a)-M1 shows that, this instrument is placed as interface of MM with GB pipes. For practical use of each schematic gate modules (symbolized cones in Fig. 6 (a)-M1), two sliding control gates are placed as Fig. 6 (b). The sliding gates act to open or close related pipe passage beside keeping the core to follow the smooth and curvy locomotion while passing through. As a functioning stages for gate modules, during function I activation, it is assumed both pipes are closed so any fluid movement and possibility of entering the core to areas are avoided. Function II and III keep an either path (e.g., MM open and GB close) open or closed. Motion of the core will depend on the function mode of gates, created fluid displacement and control valves mode. These choices to displace robot via integration of different mechanical parts, give freedom to system to have more control over itself without constraining its locomotive degrees of freedom.

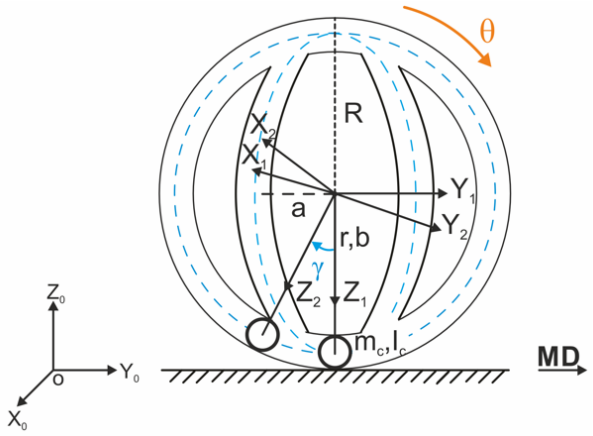

Fig. 7: Rolling motion model along O-y.

3. Movement Analysis

3.1. Analytical Criteria

Most of pendulum driven and mass displacement mechanisms in SMRs make them impracticable for internal driving units to bring the center of mass to above upper-half of the sphere. That phenomenon is avoided in this mechanism via Eq. (1), however, this instability bring three different behaviors relevant to position of the core, speed of the core and sphere. To analyze these morphologies, it is assumed that TT's core is in middle of GB so there will be no effect on diversity of center of mass related to total robot.

The graphical notations for side view of "RollRoller" is as Fig. 7. Reference frames are denoted in which $O_0 - X_0Y_0Z_0$ represents the inertial fixed reference. The moving frame connected to the center of sphere is $O_1 - X_1Y_1Z_1$, which translates only with respect to inertial fixed reference. Also, $O_2 - X_2Y_2Z_2$ is another frame attached to center like previous one but it rotates only with respect to the $O_1 - X_1Y_1Z_1$. Table 1 shows the defined variables for rolling spherical robot. We are considering that the core is traveling through the dashed line. Also, MD basically stands for main direction of "RollRoller". The core distance (r) is varied between the semi-minor (a) and semi-major (b) spaces. It is assumed that there is no slip between sphere and ground. The core unstable region is $-\frac{\pi}{2} < \gamma < \frac{\pi}{2}$, the location of $-\pi$ is assumed the stable point and $\overset{+}{-}\frac{\pi}{2}$ location looked as stable and maximum gravitational points for sphere motion. Due to similarity of $-\pi < \gamma < -\frac{\pi}{2}$ and $\frac{\pi}{2} < \gamma < \pi$, we choose the $-\pi < \gamma < -\frac{\pi}{2}$ region for our analysis. Each case gives brief summary of the core and sphere locomotion with diverse state conditions in the instability area. The core motion through MM:

Case 1: Neither the sphere nor the core has initial velocity so this results to create locomotion for sphere in opposite direction of MD as Fig. 8-1 (Initial Conditions: $\theta = 0$, $\dot{\theta} = 0$, $-\pi < \gamma < -\frac{\pi}{2}$, $\dot{\gamma} = 0$).

Table 1
Nomenclature of dynamic analysis

θ	Rolling angle of RollRoller around x axis
γ	Locomotion angle of the core
g	Gravitational acceleration
R	Sphere radius
r	Distance between the center of sphere and core
a	Semi-minor axis of GB
b	Semi-major axis of GB

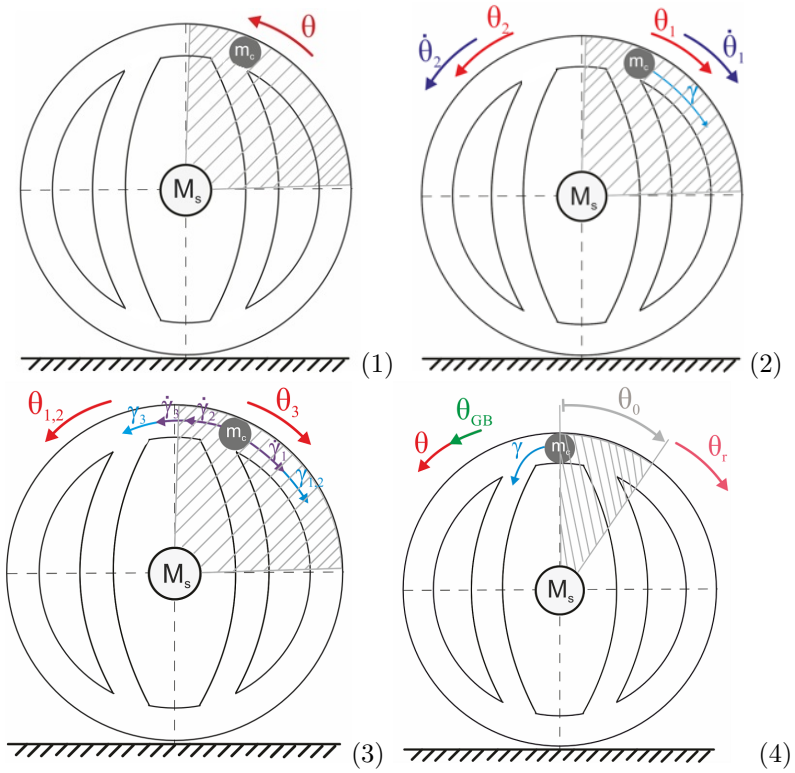

Fig. 8: (1) The sphere's motion with no initial velocity,(2) The sphere's motion with initial sphere velocity,(3) The sphere's motion with initial core velocity,(4) GB pipe core and sphere motion in "RollRoller".

Case 2: The sphere with initial velocity , leads the robot through initial response with effect of the core location. However, with given constraints, sphere follows initial velocity direction (Initial Conditions: $\dot{\theta} = 0$, $\dot{\theta}_{min} < |\dot{\theta}| <$

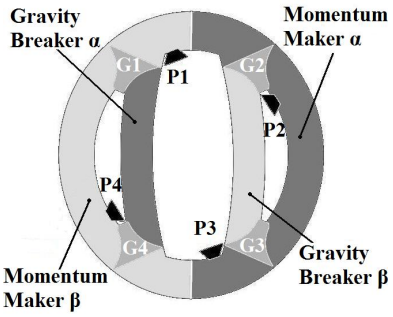

Fig. 9: Side way view and partition definition.

$\dot{\theta}_{max}$, $-\pi < \gamma < -\frac{\pi}{2}$, $\dot{\gamma} = 0$). For certain level, the sphere velocity doesn't create enough kinetic energy.

Case 3: By $\dot{\gamma}_1 > 0$ the total sphere moves counterclockwise direction with having clockwise threshold value ($\dot{\gamma}_{CT}$) for core velocity (Initial Conditions: $\theta_1 = 0$, $\dot{\theta}_1 = 0$, $-\pi < \gamma_1 < -\frac{\pi}{2}$, $0 < \dot{\gamma}_1 < \dot{\gamma}_{CT}$). When core velocity is $\dot{\gamma}_2 < 0$ till counterclockwise threshold velocity $\dot{\gamma}_{CCT}$, sphere follows the counterclockwise movement (Initial Conditions: $\theta_2 = 0$, $\dot{\theta}_2 = 0$, $-\pi < \gamma_2 < -\frac{\pi}{2}$, $\dot{\gamma}_{CCT} < \dot{\gamma}_2 < 0$). And, It is expected to give opposite responses for $\dot{\gamma}_{1,2}$, while they are exceeding the threshold velocity. $\dot{\gamma}_3$ as an example that surpass the value from $\dot{\gamma}_{CCT}$ and results robot moves in clockwise direction (Initial Conditions: $\theta_3 = 0$, $\dot{\theta}_3 = 0$, $-\pi < \gamma_3 < -\frac{\pi}{2}$, $\dot{\gamma}_3 < \dot{\gamma}_{CCT}$).

Results in section IV will show how RollRoller covers these logical hypothesis to omit the instability points. Additionally, Case 1 is true under the condition of free fall mode for the core. Therefore, either if we fix the core in its location or it has high friction between the core and pipe surfaces, total sphere will pull the core to neutralization point under M_s location. As a result, θ will turn clockwise.

Fig. 8-4 gives the sight to advantages of GB in "RollRoller", which will have direct impact on enhancing locomotion with including more freedom in robot's motion. The obtained results are shown in section IV.B.

Case 4: The core pass through the GB in the sphere with initial angle of θ_0. Resulted γ moves the sphere in counterclockwise direction with θ_{GB} which $\theta_{GB} << \theta$. θ in this case stands for locomotion of sphere if the core moves through MM (Initial Conditions: $0 \leq \theta \leq \theta_T, \dot{\theta} = 0, \gamma = k\pi, 0 \leq \dot{\gamma}$). θ_T is the boundary for sphere's slope in the unstable region. In the same way, if the total sphere has motion in clockwise direction which is in opposition with the core motion, the latest displacement θ_r after reaching the ground equilibrium point will be as Eq. (6) for both MM and GB cases.

$$\theta_r - \theta_{MM} < \theta_r - \theta_{GB} \tag{6}$$

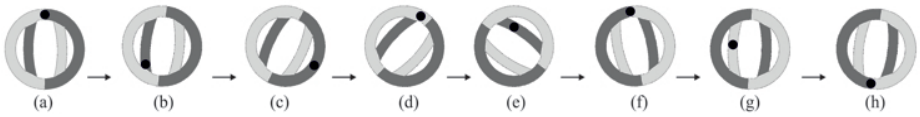

Fig. 10: The cycles of forward locomotion.

3.2. Forward Direction

The forward direction motion of robot is studied with including the gates, input ports and pipeline paths (i.e., MM and GB). As shown in Fig. 9, overall tube is divided to subparts on FT. "α" region pipes are the initiation step for locomotion and next cycle is taken by "β" region. Pn and Gn in symbolic way stand for function stages of fluid flow input/output ports and control gates, respectively.

The cylinder input and output ports are connected in series. For instance, first cylinder's two output ports are connected to P1 and P2. The gates are stated between the bi-fraction of hydraulic cylinders (e.g. $Hyd._1 \rightarrow P1 - P2$ and $Hyd._3 \rightarrow P3 - P4$).

The proposed steps are created in ideal locomotion for robot without any slippery. The relative basic control law, Algorithm 1, for perfect locomotion (Explanation in Section V) is created. The cycles in Fig. 10 are illustrated as a sample for all of possible situations. Each cycle is independent from others so the robot can stay in the specific rotation in great deal of time (i.e. Fig. 10-c) till reaches to the relatively similar form in other step.

To implement the hybrid locomotion with GB and MM interactions Algorithm 1 is designed. In the Algorithm 1, first while loop represents the time that speed of the core is equal or less than speed of the sphere (see Fig. 10-c), this behavior is considered as torque reactive form of motion which is interpreted as the pendulum driven models. Next while loop is for the special cycles that core moves from GB (see Fig. 10-d ,e and g), so the core accelerates faster and consequently causes increasing the momentum of inertia. In line 7, the η_θ and η_γ parameters are the regional constraints related to activation location for GB in which it is a main design function in Algorithm 1. Impact of this particular constraint will be evaluated in Section V on RollRoller locomotion. This is the part that system works with torque-reaction and angular momentum methods. Also, we can have only gravity-base motion by moving the core considerably fast and lock it in specific location in MM/GB pipes. It is believed, this is the first mechanism that can have all three motivation forces uniquely. As an example for the integration of control gates and input ports with the cycle of locomotion in Fig. 10 for right direction motion, the Table 2 is obtained.

3.3. Turning Motion

To have clear understanding about RollRoller's morphology on 3D plain, the turning ability of robot was studied as one of imperative degrees of freedom.

Algorithm 1 Forward Locomotion

procedure RIGHT DIRECTION MOTION($\theta, \dot{\theta}, \gamma, \dot{\gamma}$)
  Let γ's location determine the region X ▷ X is α/β
  while $0 < \dot{\gamma} \leq \dot{\theta}$ **do**
    Keep the core moving in MM of region X
  end while
  while $\dot{\theta} < \dot{\gamma}$ **do**
    if $-k\pi - \frac{\pi}{\eta_\gamma} < \gamma \leq -k\pi + \frac{\pi}{\eta_\gamma}$ and $k\pi + \frac{\eta_\theta \pi - \pi}{\eta_\theta} \leq \theta \leq k\pi + \frac{\eta_\theta \pi + \pi}{\eta_\theta}$ **then**
      Pass the core from GB of region X
    else
      Keep core moving in MM of region X
      if $(2k+1)\pi\theta \approx \gamma$ **then**
        Pass the core through the GB of region X
        Switch the region X
        return 3
      end if
    end if
  end while
end procedure

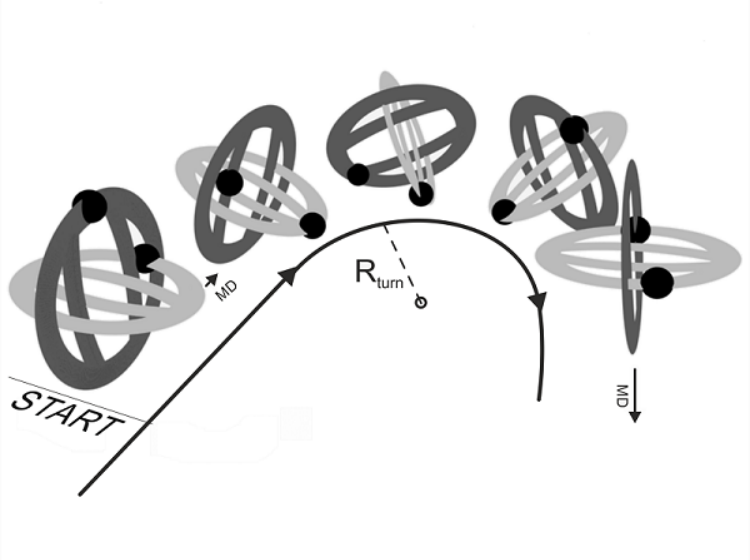

Fig. 11: Schematic of turning motion.

Table 2
Functions of forward movement

Cycle,	Gate Modules				Output Ports			
Core Loc.	G1	G2	G3	G4	P1	P2	P3	P4
a, EP	II	II	I	II	O	IT	ST	O
b, GB α	II	I	I	II	IT	O	ST	O
c, MM α	I	II	II	I	O	ST	IT	O
d, MM β	II	I	I	II	IT	O	ST	O
e, GB α	II	I	II	II	IT	ST	ST	O
f, MM β	I	II	III	III	ST	O	O	IT
g, GB β	I	III	III	I	ST	O	IT	O
h, EP	III	II	I	I	O	IT	O	ST

EP = Equilibrium Point, ST = Suction in Tube, IT = Injection in Tube, O = Off Mode, I = Closed Gate, II = Opened α and closed β, III = Opened β and closed α.

The TT core's mass is assumed with small fraction of increase δ due to deformed structure of TT (property in Eq. (1)). δ is approximated depending on the structure of TT and material of the sphere. The proposed locomotion manner for turning is developed as schematic in Fig. 11.

$$\frac{M_s}{10} + \delta \leq m_{c_{TT}} < \frac{M_s}{3} + \delta \tag{7}$$

In this form of locomotion, while FT is following the cycles in forward motion (see Fig. 10) with core velocity that tending to exceeds the sphere velocity, the TT core tend to move from MM to corner equilibrium point (intersection point of GBs and MMs) on right hand side based on the MD. By maintaining the TT core in this location through the motion period, we expect the robot to have turning with R_{turn} radius. In section V.B, the turning maneuver will be shown and compared on 3D plain with Adams/View simulation.

4. Dynamics

4.1. Forward Direction Nonlinear Dynamics

To derive the dynamics of the system, we used variables and geometry models from section III, and Fig. 12 shows the basic coordination and units of our operation.

D_{po} represents the position vector in the robot. Angular and linear velocity vectors are ω_s and V_s for total sphere, also angular velocity ω_c and linear velocity

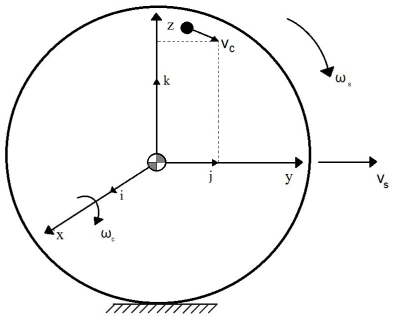

Fig. 12: The unit vectors, angular and linear velocities.

V_c are related to the core.

$$D_{po} = -a\sin(\gamma+\theta)\hat{j} - b\cos(\gamma+\theta)\hat{k} \tag{8}$$

$$\omega_s = \dot{\theta}\hat{i} \tag{9}$$

$$V_s = R\dot{\theta}\hat{j} \tag{10}$$

$$\omega_c = (\dot{\gamma}+\dot{\theta})\hat{i} \tag{11}$$

$$V_c = (R\dot{\theta} + a(\dot{\gamma}+\dot{\theta})\cos(\gamma+\theta))\hat{j} + (b(\dot{\gamma}+\dot{\theta})\sin(\gamma+\theta))\hat{k} \tag{12}$$

For obtaining the dynamic model of robot, the Lagrangian function L containing only the terms due to rotation along the O-y axis, as follows:

$$L = E_k - E_p \tag{13}$$

In Eq. (13), E_k and E_p stand for total kinetic energy and potential energy. I_s and I_c show the masses' moment of inertia for the sphere and the core.

$$L = \frac{1}{2}M_s|V_s|^2 + \frac{1}{2}I_s|\omega_s|^2 + \frac{1}{2}m_c|V_c|^2 + \frac{1}{2}I_c|\omega|^2 + m_c g d_{c-z} \tag{14}$$

Next, we just substitute parameters in Lagrangian function. This equation is mutated generally for both elliptic and circular motion as Eq. (15).

$$\begin{aligned} L = {} & \frac{1}{2}R^2\dot{\theta}^2 M_s + \frac{1}{2}I_s\dot{\theta}^2 + \frac{1}{2}I_c(\dot{\gamma}+\dot{\theta})^2 \\ & + \frac{1}{2}m_c[(R\dot{\theta} + a(\dot{\gamma}+\dot{\theta})\cos(\gamma+\theta))^2 + (b(\dot{\gamma}+\dot{\theta})\sin(\gamma+\theta))^2] \\ & + m_c g \frac{ab}{\sqrt{(a\cos(\gamma+\theta))^2 + (b\sin(\gamma+\theta))^2}}\cos(\gamma+\theta) \end{aligned} \tag{15}$$

The gravitational potential energy is adapted to have a true mode when the core is following either elliptic or circular lines in RollRoller. We assume there are distinct viscous frictions for core and sphere surfaces. The general energy dissipation function is written for Lagrangian with dependency on velocities of model.

$$P = \frac{1}{2}\sum \zeta_i \dot{q}_i^2 = \frac{1}{2}(\zeta_\theta \dot{\theta}^2 + \zeta_\gamma \dot{\gamma}^2) \tag{16}$$

The Lagrange-Euler equations for translation in O-y plain is as follows:

$$\frac{d}{dt}(\frac{\partial L}{\partial \dot{q}_i}) - \frac{\partial L}{\partial q_i} + \frac{\partial P}{\partial \dot{q}_i} = \tau_i \tag{17}$$

Where our q_i are θ and γ, respectively. Also, the input torque directly applied to the core $\tau_\gamma = bsF_{c_T}$ (s is the number of involved hydraulics) and there is no supportive/reactive force toward the total sphere $\tau_\theta = 0$.

Therefore, equations of motion for mechanical system are as :

$$\begin{bmatrix} M_{11} & M_{12} \\ M_{21} & M_{22} \end{bmatrix} \begin{bmatrix} \ddot{\theta} \\ \ddot{\gamma} \end{bmatrix} + \begin{bmatrix} N_{11} \\ N_{21} \end{bmatrix} + \begin{bmatrix} G_{11} \\ G_{21} \end{bmatrix} = \begin{bmatrix} \tau_\gamma \\ \tau_\theta \end{bmatrix} \tag{18}$$

Where parameters are defined by M_{ij} the acceleration coefficients , N_{ij} velocity dependencies and G_{ij} gravity factors, while:

$$\begin{aligned}
M_{11} &= I_c + a^2 m_c - aRm_c \cos(\gamma+\theta) + m_c \sin^2(\gamma+\theta)(b^2-a^2) \\
M_{12} &= I_c + a^2 m_c + m_c \sin^2(\gamma+\theta)(b^2-a^2) \\
M_{21} &= M_s R^2 + I_s + m_c R^2 - 2aRm_c \cos(\gamma+\theta) + Ic \\
&\quad + a^2 m_c + m_c \sin^2(\gamma+\theta)(b^2-a^2) \\
M_{22} &= I_c + a^2 m_c + m_c \sin^2(\gamma+\theta)(b^2-a^2) - aRm_c \cos(\gamma+\theta) \\
N_{11} &= -\dot{\theta}^2[aRm_c \sin(\gamma+\theta)] \\
&\quad - (\dot{\gamma}+\dot{\theta})^2[m_c \sin(\gamma+\theta)\cos(\gamma+\theta)(b^2-a^2)] \\
&\quad - (\dot{\gamma}\dot{\theta})(aRm_c \sin(\gamma+\theta)) + \zeta_\gamma \dot{\gamma} \\
N_{21} &= -\dot{\theta}^2[aRm_c \sin(\gamma+\theta)] - (\dot{\gamma}+\dot{\theta})^2[m_c \sin(\gamma+\theta)\cos(\gamma+\theta)(b^2-a^2)] \\
&\quad - (\dot{\gamma}\dot{\theta})(aRm_c \sin(\gamma+\theta)) + \zeta_\theta \dot{\theta} \\
G_{11} &= G_{21} = abm_c g[\frac{\sin(\gamma+\theta)(a^2\cos^2(\gamma+\theta)}{\dots} \\
&\quad \frac{+b^2\sin^2(\gamma+\theta)) + \frac{\sin(\gamma+\theta)\cos^2(\gamma+\theta)(b^2-a^2)}{a^2\cos^2(\gamma+\theta)+b^2\sin^2(\gamma+\theta)}}{a^2\cos^2(\gamma+\theta) + b^2\sin^2(\gamma+\theta)}]
\end{aligned} \tag{19}$$

We orientate the nonlinear dynamics in this subsection in Eq. (18) as second order equations to help us to have better view over the system.

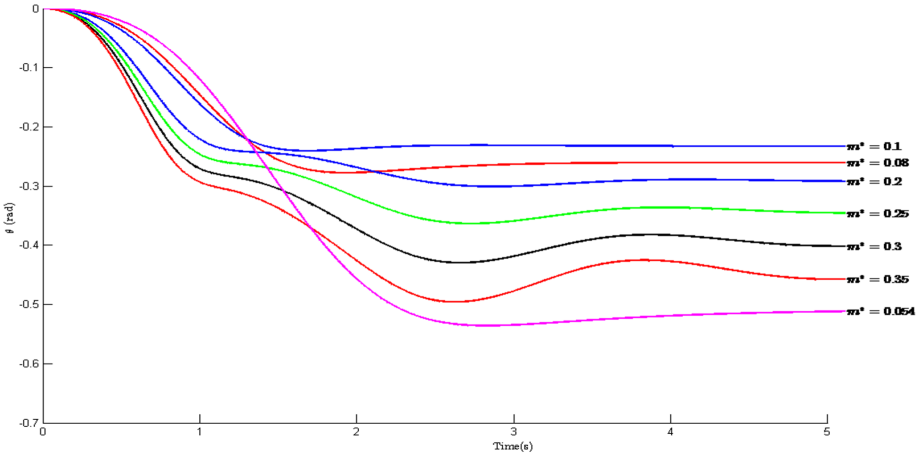

Fig. 13: Instability behavior in motion of sphere for different mass ratios.

Table 3
Data of RollRoller's dynamic variables

Variable	Value	Variable	Value
g	$9.8\ \ m/s^2$	b	$0.131\ \ m$
M_s	$1\ \ kg$	a	$0.0450\ \ m$
m_c	$0.25\ \ kg$	$I_{c_{MM}}$	$0.0402\ \ kg.m^2$
ζ_θ	0.2	$I_{c_{GB}}$	$7.7440 \times 10^{-4}\ \ kg.m^2$
ζ_γ	< 0.1	I_s	$0.0140\ \ kg.m^2$
R	$0.145\ \ m$		

4.2. Dynamics Results

We analyze the dynamics for two basic points; first, about verifying the proposed criteria in section III for omitting the instability point. Second, to show the efficiency of proposed algorithm. The derived nonlinear dynamics in Eqs. (18)-(19) are solved via ODE45 solver [20, 21] in Matlab. We used variables from Table 3 in evaluating the motion of system.

The inertia coefficients of sphere and core in MM and GB pipes are:

$$\begin{aligned} I_s &= \frac{2}{3} M_s R^2 \\ I_{c_{MM}} &= \frac{2}{5} m_c b^2 \\ I_{c_{GB}} &= \frac{2}{5} m_c (\frac{a+b}{2})^2 \end{aligned} \tag{20}$$

The average of semi-minor and semi-major distance has been substituted in

order to estimate and settle the momentum of inertia in the system to its true value when entering to GB path. The viscous friction of sphere is adapted to the environment that is approximately on an even terrain. The core displacement also has the minimum dissipation energy by assuming the frictionless surface between core and interior part of pipe.

4.2.1. m^* Range Validation

As it is seen from inequality (1), to obtain the applicable domain of mass ratio for sphere and core, we analyze the dynamics in $X_0 = [\theta \quad \dot{\theta} \quad \gamma \quad \dot{\gamma}] = [0 \quad 0 \quad -\frac{3\pi}{2} \quad 0]$ initial conditions with no input torque. Also the dissipation coefficients for core and sphere are assumed $\zeta_\gamma = 0.01$ and $\zeta_\theta = 0.2$. As it is seen from Fig. 13, the stability domain is limited between 0.1 - 0.3. For values over lower and upper limits system follows abnormal displacement along the axis. Also, due to considerable high amplitude ripples after 0.3 mass ratio the results become uncontrollable. The chosen value for mass of the core and $m*$ ($m_c = 0.25$ kg and $m* = 0.25$) in Table 3 is the value with minimum overshoots (nearly 5%) and settling time (5.2 sec) which are the characteristics of under-damped stable system for this study.

4.2.2. Analytical Criteria

We analyze the MM in instability region and effect of GB as section III.A through dynamics. The viscosity of core is $\zeta_\gamma = 0.01$ for first three cases (MM parts) and in Case 4 the viscous friction is increased to $\zeta_\gamma = 0.075$ to have clearer view over velocities due to defined dynamic constraint in inertia coefficient of GB path ($I_{c_{GB}}$).

Case 1: The plot series in Fig. 14-a demonstrates the results for 6 different values of γ_0 in region of instability ($-\pi < \gamma_0 \leq -\frac{\pi}{2}$). Mobility starts with basic initial condition $X_0 = [\theta \quad \dot{\theta} \quad \gamma \quad \dot{\gamma}] = [0 \quad 0 \quad \gamma_0 \quad 0]$. The red value ($\gamma_0 = -\frac{\pi}{2}$ rad) is the critical point of motion since it aims the sphere to move in forward direction and also this is the place in which creates similar movement in lower half of sphere ($-\frac{\pi}{2} \leq \gamma_0 \leq 0$). We saw as initial location of the core climbs up, the total movement of sphere became backward. The $\gamma_0 = -\frac{5\pi}{6}$ rad (Fig. 14 black line) is illustrating, displacement ratio jumps when the value gets nearer to the upper equilibrium point $\gamma_0 = -\pi$ rad in stationary condition.

Case 2: The system is excited with different values of sphere's initial velocities,$0 \leq |\dot{\theta_0}| \leq \pi$. The core begins from fixed point in unstable region, $\gamma_0 = -\frac{3\pi}{4}$ rad ($X_0 = [0 \; \dot{\theta_0} \; -\frac{3\pi}{4} \; 0]$). RollRoller robot follows direction of motion relative to sphere's speed. However, The range of locomotion or efficiency of movement interestingly is integrated. There is kinetic clue in movement, robot's core location over time depends to sphere's speed because the core is moving in circular path. As a result, it can be said the maximum displacement can be approximated as Eq. (21) in this case. This relation is not unit base relation.

$$\dot{\theta} \simeq \frac{\gamma}{g} \tag{21}$$

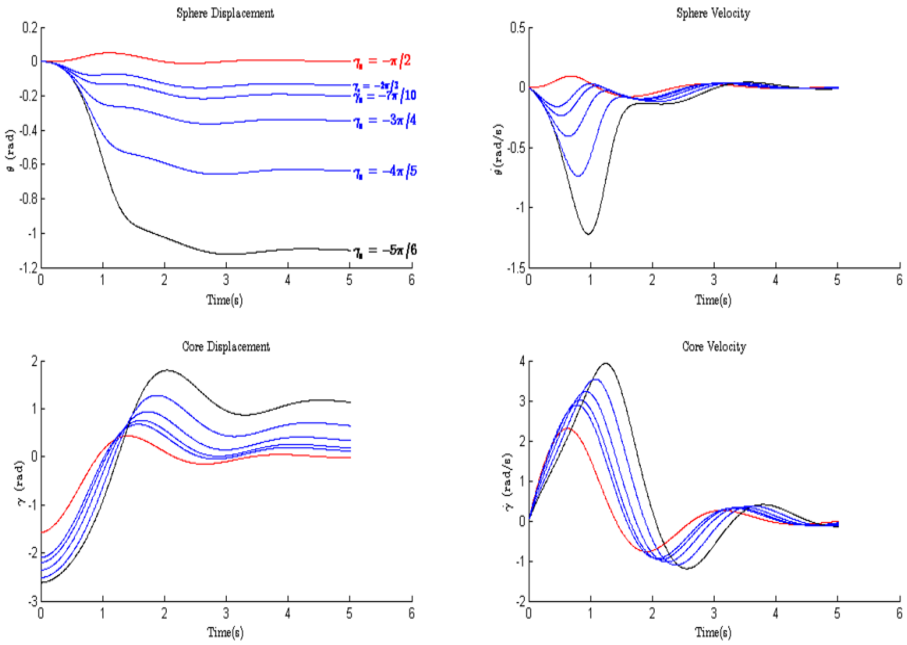

(a)

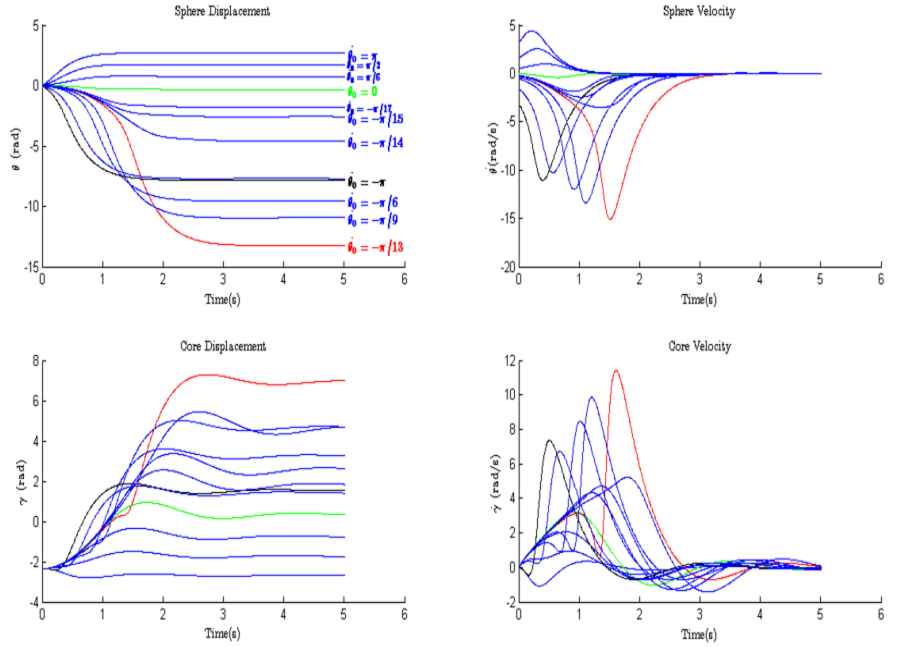

(b)

Fig. 14: (a) The case 1 motion and speed plots for $-\pi \leq \gamma_0 < -\frac{\pi}{2}$, $X_0 = [0 \quad 0 \quad \gamma_0 \quad 0]$ values, (b) the case 2 motion and speed plots for $0 \leq |\dot{\theta_0}| \leq \pi$ values, $X_0 = [0 \quad \dot{\theta_0} \quad -\frac{3\pi}{4} \quad 0]$.

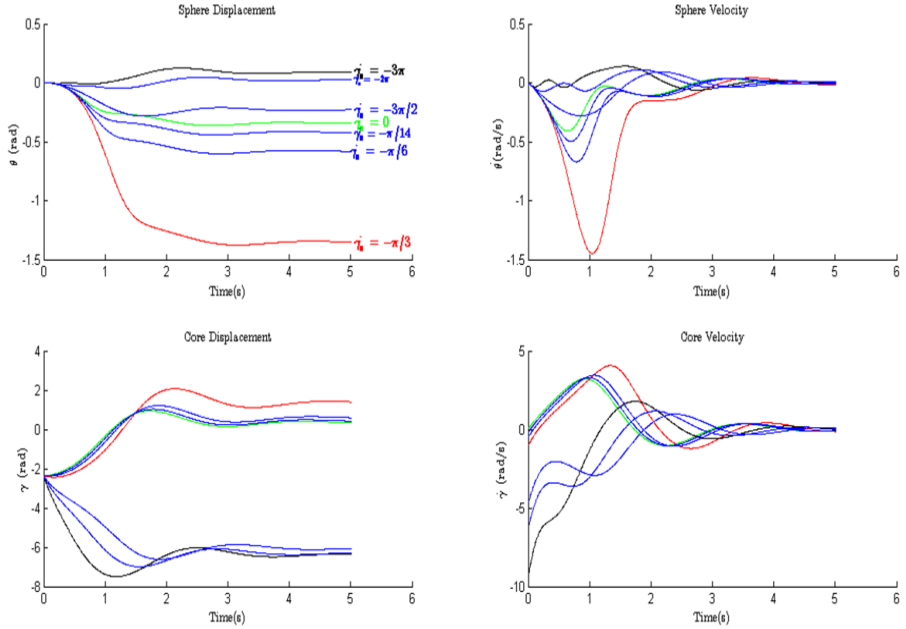

(a)

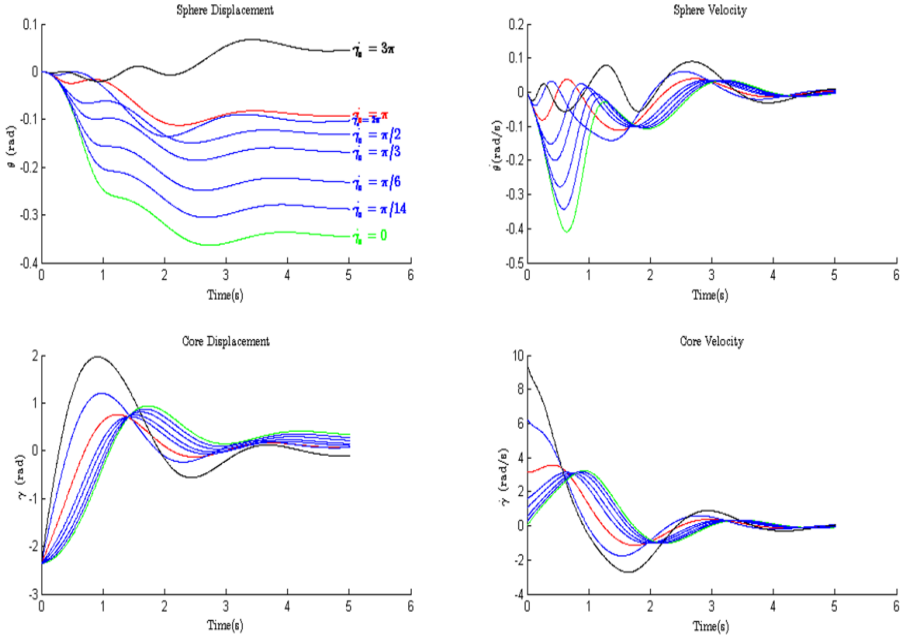

(b)

Fig. 15: The case 3 movement and velocity plots for $-3\pi \leq \dot{\gamma}_0 < 3\pi$ values, $X_0 = [0 \quad 0 \quad -\frac{3\pi}{4} \quad \dot{\gamma}_0]$. Note that the black, red and green lines stand for maximum initial input core velocity in both sides, unexpected nonlinear manner and no input velocity as reference , respectively.

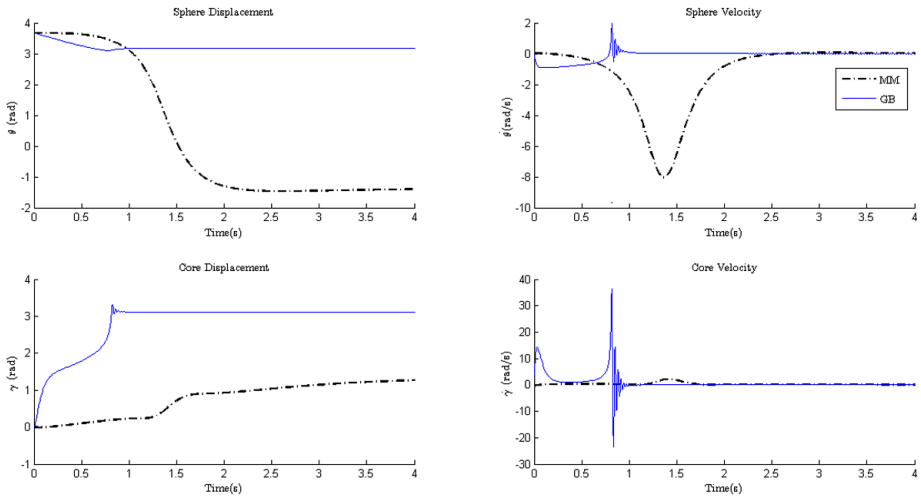

Fig. 16: The GB and MM behavior with initial condition as $X_0 = [-\pi \; -\frac{\pi}{6} \; 0.1 \; 0 \; -\frac{\pi}{8}]$

Case 3: Illustrating how SMR is able to maneuver despite the condition of actuator is one of the essential points. Fig. 15 shows locomotion of sphere with different velocity responses in both directions. The initial states were $X_0 = [0 \;\; 0 \;\; -\frac{3\pi}{4} \;\; 0 \leq \dot{\gamma}_0 \leq 3\pi]$. In the state that robot contains counterclockwise velocity for certain level ($0 \leq \dot{\gamma} \lessapprox -2\pi$) it produces backward locomotion. When the velocity exceeds this property, the -2π rad/s, sphere's locomotion follows the opposite direction of same axis. However, specific constraint is been created for cases that core velocity is positive because the core location is at $\gamma_0 = -\frac{3\pi}{4}$ rad. Although, we inject positive velocity to core and expect clockwise turning for sphere (see Fig. 15-b), the outcomes are showing this only possible when core's velocity exceeds the 2π rad/s. And, around the values over the π rad/s it saturates around the red line ($\dot{\gamma}_0 = \pi$ rad/s) in Fig. 15.

Case 4: As it was obvious from Fig. 15, in unstable regions, the problem of limiting the velocity of core (requiring sudden change of velocity parallel to clear negative impacts) to keep motion completely concentrated on one direction is become hard task. Fig. 16 gives an example point from case 4 and shows how GB outperforms itself and doesn't create certain backward locomotion. The most realistic results with containing impacts will be explained and shown in Section V. The Offset between the MM used model and GB is:

$$Offset = |\theta_{MM_{setteled}}| - |\theta_{GB_{setteled}}| = 4.82 \; rad \tag{22}$$

Also, the negative velocity that sphere carries, is totally omitted in GB. In this motion, core with fix circular turn in MM can create fluctuation in sphere displacement and also its velocity. Furthermore, the created ripple in core velocity at around $t = 0.8$ sec is coming from estimation of inertia as we explained before. lastly, our algorithm in Section III.B can be seen as satisfying proposal for

forward direction cycle with GB inclusion during high proportional core's speed (Fig. 10 cycles b,d and g).

4.2.3. Forward Locomotion

To see the compact manner of RollRoller by using the derived nonlinear Eqs. (18)-(20), the system has been taken to hybrid state. From the Section III.B, we consider the motion has all state properties from cycle a to h in Fig. 10 except cycle e. Cycle e only occurs in cases where core velocity is changing instantly. For hybrid model of GB and MM motion, we stem position control method from Algorithm 1 particularly in $\dot{\theta} < \dot{\gamma}$ condition. In our experiment η_θ and η_γ are approximately $\frac{\pi}{12}$ rad. However, We orientate the algorithm for implementation with over-writing its dependency on the sinusoidal locational form to have more freedom in our parameters variety. The constraints for line 7 are mutated as follows:

$$\begin{aligned}\{\cos(\theta) \leq -0.95 \ \ and \ \ \sin(\theta) \geq -0.2 \ \ and \ \ \dot{\theta} \geq 0 \ \ and \\ \dot{\gamma} \leq 0 \ \ and \ \ \cos(\gamma) \geq 0.9 \ \ \sin(\gamma) \leq 0.2 \ \} \ \ OR \\ \{\cos(\theta) \geq 0.95 \ \ and \ \ \sin(\theta) \leq 0.2 \ \ and \ \ \dot{\theta} \geq 0 \ \ and \\ \dot{\gamma} \leq 0 \ \ and \ \ \cos(\gamma) \leq -0.9 \ \ and \ \ \cos(\gamma) \geq -0.2\}\end{aligned} \tag{23}$$

Also, Line 11 is transformed to:

$$\begin{aligned}\{|\cos(|\gamma|)| \leq 0.9 \ \ and \ \ \sin(|\gamma|) \leq 0\} \ OR \\ \{|\cos(|\gamma|)| \leq 0.9 \ \ and \ \ \sin(|\gamma|) \geq 0\}\end{aligned} \tag{24}$$

Eqs. (23)-(24) are designed for both α and β regions. Also, sphere's small differential degree in clockwise direction in Algorithm 1 as shown in mutated equations is constrained by our design property that remove negative impacts in RollRoller motions when GB interacts (see Section V results). The hybrid integration of MM and GB pipes are defined by creating two series of core-sphere distances and viscous frictions. The viscous frictions of MM are $\zeta_{\theta_{MM}} = 0.2$ and $\zeta_{\gamma MM} = 0.01$. Also, $\zeta_{\theta_{GB}} = 0.2$ and $\zeta_{\gamma GB} = 0.01$ are the GBs' viscous frictions. Fig. 17 shows our implemented algorithm for this motion with $X_0 = [0 \ \ 0 \ \ -\frac{\pi}{2} \ \ 0]$ initial conditions. The step size of ODE45 solver is chosen $T = 0.01$. The input torque τ_γ to core is -0.075 N·m in counterclockwise direction in our experiment to satisfy Eq. (5).

Initially, RollRoller passes the core through GB pipe and the core in $\gamma_{jump_1} = -6.2304$ rad leaves GB with $\dot{\gamma}_{jump_1} = -69.8284$ rad/s velocity. On the other side, pendulum-driven models (e.g., [4, 5, 8, 10, 9, 11, 22, 19]) with given characteristics behave the locomotion by only circling the core with concave curve in MM. Our robot's velocity jump leads the motion from MM with semi-linear displacement. In the next step, the core entered GB for a second time ($\gamma_{jump_2} = -31.7397$ rad and $\theta_{jump_2} = 2.9681$ rad), After exceeding $\dot{\theta} < \dot{\gamma}$.

The second jump carries the $X = [3.2648 \;\; 9.9830 \;\; -34.7005 \;\; -83.9019]$ states to MM pipe. This iteration continues for next steps. However, This is position control for certain locomotion. For higher speeds, there must be integrated velocity control over the core. Simultaneously, robot to maintain/increase its speed, it may keep the core in GB for certain time. This limitation can come to sight after certain iterations.

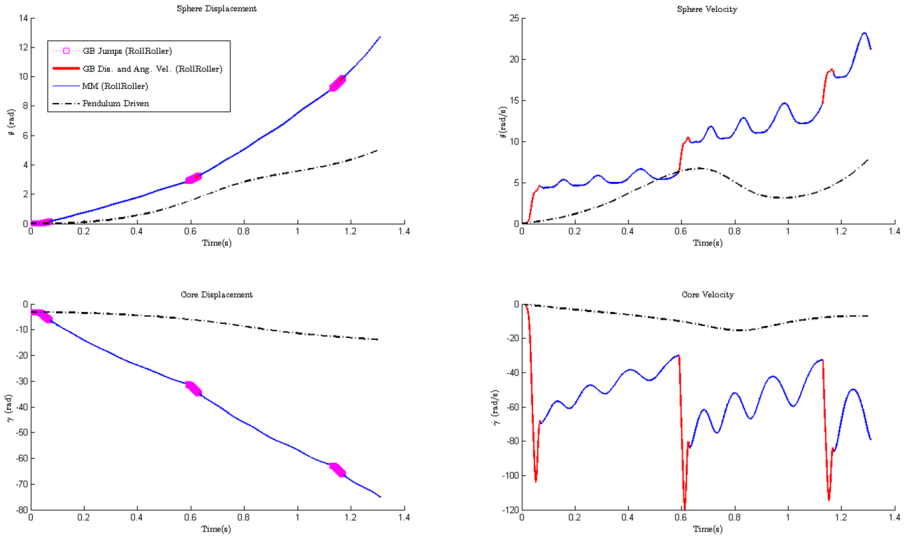

Fig. 17: The pendulum model which designed with our parameters and RollRoller maneuver in forward direction ,with $X_0 = [0 \;\; 0 \;\; -\frac{\pi}{2} \;\; 0]$ initial conditions.

The advantages of our model are visible from mathematical model results. The overall displacement without complete feedback control can create exponential increase in comparison to its own counterparts.

$$Offset = |\theta_{RollRoller}| - |\theta_{PendulumDriven}| = 7.713 \; rad \tag{25}$$

Also, the displacement is free from any swing during the time. We see the velocity response of our robot is rectified in negative part of sinusoidal. There is minor velocity diversity during the motion. The peak in core velocity during jump comes from low dissipation energy which can be minimized with feedback control within GB path. We didn't have a look to the motion of sphere in low velocities $\dot{\theta} \geq \dot{\gamma}$ since this motion is similar to its counterparts that actuates with depending to gravitational and torque-reaction forces.

5. Numerical Simulation

To validate the derived nonlinear equations and get more insight to motion of RollRoller, the model is implemented to Adams/View simulation space in Fig.

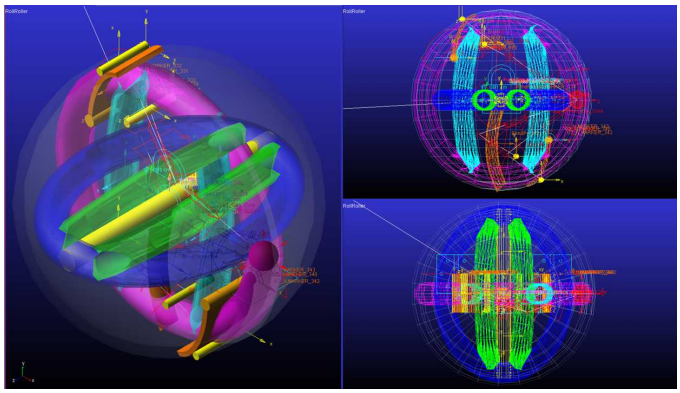

Fig. 18: Adams/View RollRoller model.

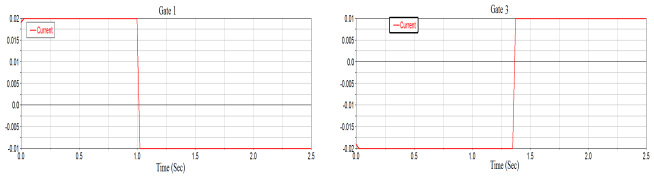

Fig. 19: Force verses time for gates functioning period.

18. We basically designed and imported the Solidworks model of RollRoller by utilizing the informations from Table 3.

Our created model is estimated the superfluid circulation to the pendulum-like pusher to move the core. The friction property of sphere-ground also is adjusted from dissipation function in mathematical model as 0.6 for static friction and 0.3 for dynamic friction. This friction coefficient indicates the existence of certain slippage between the sphere and plain surfaces which makes the model more realistic in application. The mass of spherical shell is considered about 900 *grams* and rest of weight is spread around the parts to have homologous mass distribution over system. We assume the core and pipe surfaces are in minimum friction (approx. 0). Two of the control gates are designed with curvy model to minimize the reaction force when core pass this object. In this simulation, control gates are inspired from Fig. 6 (b) with difference that they are articulating instead of sliding (two sliding gates are replaced with one articulating gate) for simplicity. Lastly, the FT core's mass is designed by means of Eq. (1) as same as dynamic model (0.25 kg).

5.1. Exceeded Core Velocity ($\dot{\theta} < \dot{\gamma}$)

To see and compare our model with and without the algorithm, we design simulated RollRoller to move in compact form in $\dot{\theta} < \dot{\gamma}$ condition. We excite the pusher with 0.35 N which creates clockwise torque to push the core. The functioning period for both gates 1 and 3 are like in Fig. 19. These step inputs

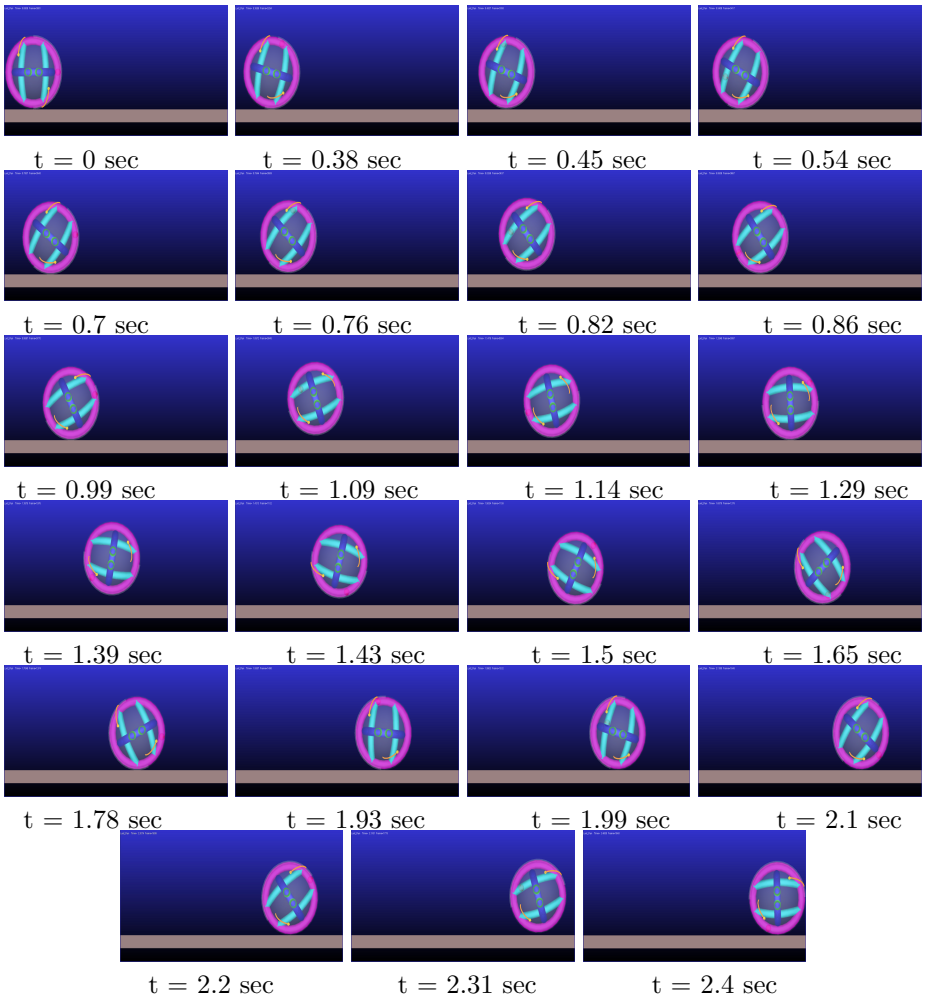
t = 0 sec
t = 0.38 sec
t = 0.45 sec
t = 0.54 sec
t = 0.7 sec
t = 0.76 sec
t = 0.82 sec
t = 0.86 sec
t = 0.99 sec
t = 1.09 sec
t = 1.14 sec
t = 1.29 sec
t = 1.39 sec
t = 1.43 sec
t = 1.5 sec
t = 1.65 sec
t = 1.78 sec
t = 1.93 sec
t = 1.99 sec
t = 2.1 sec
t = 2.2 sec
t = 2.31 sec
t = 2.4 sec

Fig. 20: Captured frames in forward locomotion in Adams/view simulation within 2.5 sec.

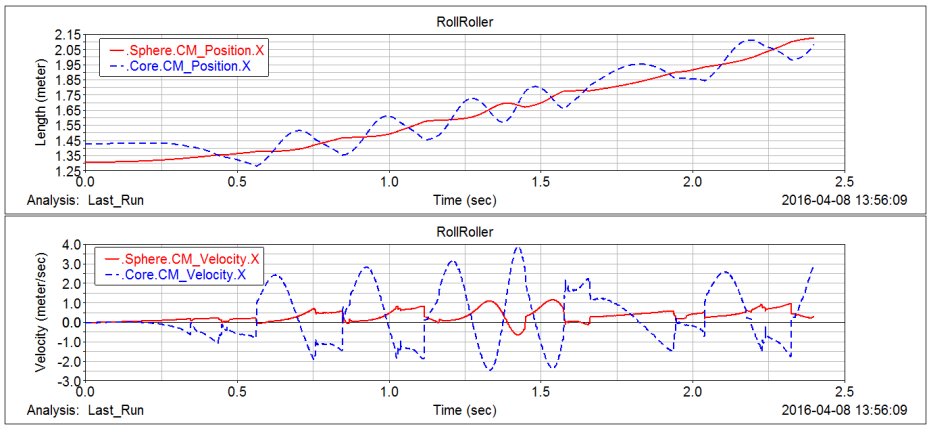

Fig. 21: Movement and velocity of core and sphere for 2.5 sec.

help us to achieve the relative response in examining the Algorithm 1. Our SMR begins the locomotion with $X_0 = [0 \;\; 0 \;\; -\frac{\pi}{2} \;\; 0]$ initial conditions. In Fig. 20, we have captured some frames after running the Adams/View simulation.

It is observed, RollRoller moves in linear form during the transient state before t = 0.5 sec (see Fig. 21). In around $0.45 - 0.54$ sec intervals, core passes the GB to prevent the negative velocity and backward locomotion of sphere. However, the rectified velocity can be seen more clearly about 0.75 sec when GB is used for a second time. After letting the core to circulate by algorithm, we change the function of gates to open just MM pipes. Between 1.09 to 1.5 sec, the fluctuation is appeared in core displacement and velocity, consequently. In the next stage, we set back the algorithm to observe the morphology in different state conditions after 1.5 sec. Therefore, we first let core enter GB in the beginning with $0 < \theta_e < k\pi + \frac{\pi}{3}$ various conditions and then we change it to $k\pi - \frac{\pi}{3} \leq \theta_e < 0$. The results show us although we succeed in our proposal method in this example, the advantages and sensitivity of algorithm become more clear. Y axis jumps and decrease in conserved velocity of sphere are relative to the time that core passes from MM to GB through gates.

It is observed, as we proposed the algorithm to let robot passes the core from the GB when sphere is in $0 < \theta_e < k\pi + \frac{\pi}{3}$, firstly it stops the sphere to have backward motion. Secondly, as we tend to have sharper degrees (i.e. $k\pi + \frac{\pi}{3} < \theta_e < k\pi + \frac{\pi}{2}$) in sphere and simultaneously requires the core to pass the GB in these locations, there are relative jumps in y axis in RollRoller (Fig. 22). Therefore, the defined constraints in Algorithm 1 matches the optimized movement criteria. Moreover, entering the core to GB in $k\pi - \frac{\pi}{3} \leq \theta_e < 0$ locations creates smoother motion in x axis but it has negative impacts in velocity of robot in which decreases our positive locomotion (see Fig. 21, after 1.6 *sec*). The reason is the created reaction force that gates gives to total sphere when core pases GB. Next, the difference of mathematical model and simulated SMR in the acceleration become more understandable.In this simulation, We are

not able to see major increase in velocity of RollRoller since the imperfect form of curvy gates cancel the great deal of energy by injecting the reaction force to pusher (pusher is connected to sphere's body via revolute joint). This problem would be nominal if the core was excited with fluid circulation by cylinders.

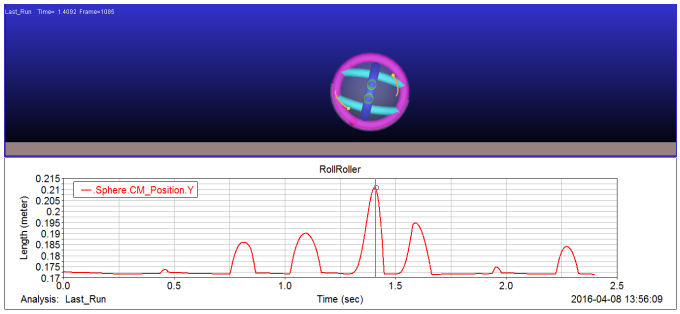

Fig. 22: RollRoller jumps in played simulation. Note: The 21 cm as the largest value before 1.5 sec stands for robots without the algorithm 1.

Fig. 23: RollRoller jumps in played simulation. Note: 3.8 cm value before 1.5 sec highlights the largest jump during the deactivation of RollRoller's designed motion algorithm (Algorithm 1).

We see from Fig. 22-23 that our translational momentum in y axis and range of jumps (Fig. 22: $t_1 = 0.45$ sec , $y_1 = 0.18$ cm and $t_2 = 1.95$ sec , $y_2 = 0.27$ cm) worked out perfectly inside the created algorithmic constraints. Moreover, The greatest deal of momentum energy diversity and highest jumps happens during time (t = 1.4 sec) that robot's algorithm is deactivated.

5.2. Turning Locomotion

To see the robot when it's TT's section activated for 3D locomotion, we prepare the system for turning action as an example. By citing the Section III.C, the TT core's mass is 0.26 kg with same body properties as FT core. As an important structural characteristic before the simulation, the TT core is blocked in same place as Fig. 11 within $\pm$ 1 cm space. Also to prevent

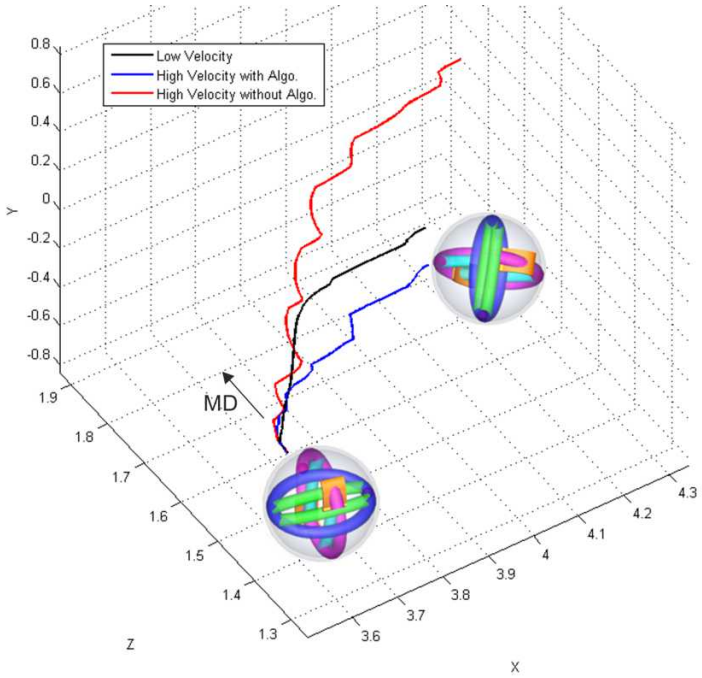

Fig. 24: Robot during its turning action for three methods. Note: The low velocity (black line), high velocity with algo. (Blue line) and high velocity without algo. (red line) stand for low core's speed ($\dot{\theta} \geq \dot{\gamma}$), high core's speed with algorithm ($\dot{\theta} < \dot{\gamma}$) and high core's speed without algorithm ($\dot{\theta} < \dot{\gamma}$).

severe vibration in robot while it is turning, the damping and stiffness factors of contact between blockers and TT core are 10^4 N·s/m and 10^3 N/m, respectively.

We see the results in Fig. 24 for three separate scenarios. The simulation is run for $t = 1.7$ sec with 0.0012 step size. When RollRoller wants to have turn in low velocity ($F_{c_T} > F_{c_{Max}}$), the behavior is smooth and lets it to have 90^o turn without any swing (pusher input force $= -0.24$ N). However, by exceeding the core speed depending to sphere's speed (pusher input force $= -0.35$ N), we achieve resealable movements. Serious swings take place in its transient response while our algorithm is deactivated (i.e., pendulum driven models general problems) but motion with algorithm gives us clear explanation about ability to control the sphere in higher velocities. Not only robot can reach the required position in lesser time but also it does not contain fluctuation in its locomotion. The only problem as explained in Section V.A is the imperfect gates that wastes some energies when core carrying, becomes a deterrent force to sphere via pusher.

6. Conclusion

In this paper, we introduce mechanism of RollRoller as a novel SMR that works with high density fluid circulation. Instead of having mechanisms that solely rely on single or integration of previous models for their actuations, RollRoller robot includes all motivation methods in a single unique model with 4 degrees of freedom. We omit the common unstable region of pendulum-like SMR drivers with our mechanism and validate the results via derived nonlinear dynamics. By using the gained insight to the locomotion manners of RollRoller, we show how our proposed algorithmic motion control outperforms through nonlinear dynamics. Next, we import our model to Adams/View simulator and observe how backward jumpings are removed during high velocities beside the improvements in their fluctuations. Our results demonstrate that RollRoller like wheeled robots, is now able to accelerate in the field which solves the another main problem in ball shape robots. To illustrate the one of degrees of freedom and strengthen the proposed motion planning in 3D plain, we check the performance of RollRoller while it is turning. Despite some simulation restrictions that come from our actuators, we see that RollRoller is able to have about 90^o turn in most linear and the fastest manner. Although, these results raise an interesting point about spherical mobile robots, they show requirements in advancing simulation space for hydraulic application. Also, Our future primary aim is to create a general non-holonomic control formulation beside velocity stabilizer for the system.

Acknowledgment

The authors would like to thank Dr. Larissa Khodadadi and Negar Esmaeilzadeh Kandjani for their contributions in preparing this paper.

References

References

[1] R. H. Armour, J. F. Vincent, Rolling in nature and robotics: A review, Journal of Bionic Engineering 3 (4) (2006) 195 – 208. doi:10.1016/S1672-6529(07)60003-1.

[2] A. Behar, J. Matthews, F. Carsey, J. Jones, Nasa/jpl tumbleweed polar rover 1 (2004) 395. doi:10.1109/AERO.2004.1367622.

[3] Z. Li, J. Canny, Motion of two rigid bodies with rolling constraint, IEEE Trans. Robot. Autom. 6 (1) (1990) 62–72. doi:10.1109/70.88118.

[4] A. Halme, T. Schonberg, Y. Wang, Motion control of a spherical mobile robot 1 (1996) 259–264. doi:10.1109/AMC.1996.509415.

[5] A. Bicchi, A. Balluchi, D. Prattichizzo, A. Gorelli, Introducing the "spherical": an experimental testbed for research and teaching in nonholonomy 3 (1997) 2620–2625. doi:10.1109/ROBOT.1997.619356.

[6] J. Brown, H.B., Y. Xu, A single-wheel, gyroscopically stabilized robot 4 (1996) 3658–3663. doi:10.1109/ROBOT.1996.509270.

[7] S. Bhattacharya, S. Agrawal, Spherical rolling robot: a design and motion planning studies, IEEE Trans. Robot. Autom. 16 (6) (2000) 835–839. doi:10.1109/70.897794.

[8] A. H. J. A, P. Mojabi, Introducing august: a novel strategy for an omnidirectional spherical rolling robot 4 (2002) 3527–3533. doi:10.1109/ROBOT.2002.1014256.

[9] G. C. Schroll, Design of a spherical vehicle with flywheel momentum storage for high torque capabilities, Master's thesis, Massachusetts Institute of Technology, Cambridge (2008).

[10] D. Liu, H. Sun, Q. Jia, Stabilization and path following of a spherical robot (2008) 676–682doi:10.1109/RAMECH.2008.4681358.

[11] M. Ishikawa, R. Kitayoshi, T. Sugie, Volvot : A spherical mobile robot with eccentric twin rotors (2011) 1462–1467doi:10.1109/ROBIO.2011.6181496.

[12] C. Wei-Hsi, C. Ching-Pei, Y. Wei-Shun, L. Chang-Hao, L. Pei-Chun, Design and implementation of an omnidirectional spherical robot omnicron (2012) 719–724doi:10.1109/AIM.2012.6266036.

[13] G. Oriolo, M. Vendittelli, A framework for the stabilization of general nonholonomic systems with an application to the plate-ball mechanism, IEEE Trans. Robot. 21 (2) (2005) 162–175. doi:10.1109/TRO.2004.839231.

[14] A. Morinaga, M. Svinin, M. Yamamoto, A motion planning strategy for a spherical rolling robot driven by two internal rotors, IEEE Trans. Robot. 30 (4) (2014) 993–1002. doi:10.1109/TRO.2014.2307112.

[15] V. Muralidharan, A. D. Mahindrakar, Geometric controllability and stabilization of spherical robot dynamics, IEEE Trans. Automat. Control 60 (10) (2015) 2762–2767. doi:10.1109/TAC.2015.2404512.

[16] M. Svinin, S. Hosoe, Motion planning algorithms for a rolling sphere with limited contact area, IEEE Trans. Robot. 24 (3) (2008) 612–625. doi:10.1109/TRO.2008.921568.

[17] F. Alouges, Y. Chitour, R. Long, A motion-planning algorithm for the rolling-body problem, IEEE Trans. Robot. 26 (5) (2010) 827–836. doi:10.1109/TRO.2010.2053733.

[18] A. V. Borisov, A. A. Kilin, I. S. Mamaev, How to control chaplygin's sphere using rotors, Reg. and Chaotic Dynam. 17 (3) (2012) 258–272. doi:10.1134/S1560354712030045.
URL http://dx.doi.org/10.1134/S1560354712030045

[19] E. Kayacan, E. Kayacan, H. Ramon, W. Saeys, Adaptive neuro-fuzzy control of a spherical rolling robot using sliding-mode-control-theory-based online learning algorithm, IEEE Trans. Cybern. 43 (1) (2013) 170–179. doi:10.1109/TSMCB.2012.2202900.

[20] J. Dormand, P. Prince, A family of embedded runge-kutta formulae, J. Comput. Appl. Math. 6 (1) (1980) 19–26. doi:http://dx.doi.org/10.1016/0771-050X(80)90013-3.

[21] L. F. Shampine, M. W. Reichelt, The matlab ode suite, SIAM J. Scien. Comput. 18 (1) (1997) 1–22. doi:10.1137/S1064827594276424.

[22] S. Mahboubi, M. Seyyed Fakhrabadi, A. Ghanbari, Design and implementation of a novel spherical mobile robot, J. Intell. Robot. Sys. 71 (1) (2012) 43–64. doi:10.1007/s10846-012-9748-8.